Chiral extrapolation of light resonances from one and two-loop unitarized Chiral Perturbation Theory versus lattice results

J. R. Peláez and G. Ríos
Dept. Física Teórica II. Universidad Complutense, 28040, Madrid. Spain.

We study the pion mass dependence of the $\rho(770)$ and $f_0(600)$ masses and widths from one and two-loop unitarized Chiral Perturbation Theory. We show the consistency of one-loop calculations with lattice results for the M_ρ, f_π and the isospin 2 scattering length a_{20}. Then, we develop and apply the modified Inverse Amplitude Method formalism for two-loop ChPT. In contrast to the $f_0(600)$, the $\rho(770)$ is rather sensitive to the two-loop ChPT parameters – our main source of systematic uncertainty. We thus provide two-loop unitarized fits constrained by lattice information on M_ρ, f_π, by the $q\bar{q}$ leading $1/N_c$ behavior of the ρ and by existing estimates of low energy constants. These fits yield relatively stable predictions up to $m_\pi \simeq 300-350$ MeV for the ρ coupling and width as well as for all the $f_0(600)$ parameters. We confirm, to two-loops, the weak m_π dependence of the ρ coupling and the KSRF relation, and the existence of two virtual $f_0(600)$ poles for sufficiently high m_π. At two loops one of these poles becomes a bound state when m_π is somewhat larger than 300 MeV.

PACS numbers:

I. INTRODUCTION.

The spectrum of the lightest meson resonances in QCD, particularly the scalars, is still not well understood from first principles. Lattice QCD can provide, in principle, a rigorous way to extract non-perturbative quantities from QCD, but current calculations are hindered by difficulties, like those associated to disconnected graphs, and their need to use relatively high quark masses, so that appropriate extrapolation formulas are needed. In Ref.[1] the quark mass dependence of the mass and width of the ρ and σ (or $f_0(600)$) mesons was predicted. Both the mass and width were obtained from the poles in $\pi\pi$ scattering amplitudes generated with the one-loop Inverse Amplitude Method (IAM) [2–4]. The IAM is obtained from a dispersion relation based on analyticity, elastic unitarity and Chiral Perturbation Theory (ChPT) [6]. The relation between m_π and the quark mass is well known and model independent within ChPT, which also provides the correct m_π dependence of low energy scattering amplitudes up to a given chiral order. There were, however, two aspects in which the calculation in [1] needed further improvement: on the one hand, at that time we were only able to compare with a single lattice $\rho(770)$ mass calculation at one value of m_π. On the other hand, we presented a calculation up to one-loop, namely next to leading order (NLO) unitarized ChPT, so that the main source of systematic uncertainty, coming from higher orders, could not be estimated.

In this paper we address these two issues. First, in the next subsection we briefly review the notation and the one-loop unitarization formalism used in [1]. Next, in Sect.II we show the good agreement of the one-loop previous calculation with several lattice group results, not only for the $\rho(770)$ mass at many values of the pion mass, but also for f_π and the isospin-2 scattering length pion mass dependence. In addition, since ref.[1] provided a strong indication that the $\rho\pi\pi$ coupling was almost quark mass independent, we perform here an explicit calculation of the ρ and σ couplings from the residues of their associated poles, confirming the very weak dependence of the ρ pole on the pion mass, in sharp contrast with the σ behavior. Next, in Sect.III, we present our calculations for unitarized two-loop Chiral Perturbation Theory. Unfortunately, the dispersive formalism used in [1], which is a modification of the well known IAM [2, 3] that incorporates correctly the Adler zeros, was developed in [4] in detail only for the one-loop case. Thus, in subsection III A we provide the justification and the expression that modifies the IAM to incorporate the Adler zeros correctly up to two loops. Next, in subsection III B we discuss the large uncertainties in the two-loop low energy constants, that will dominate our systematic errors, particularly for the $\rho(770)$, as explained in subsection III C. Therefore, to ensure the correct mass dependence, in subsection III D we fit these constants not only to experimental data but also to the existing lattice results with the additional constraint of respecting the $q\bar{q}$ leading order $1/N_c$ behavior for the ρ as well as existing estimates of the low energy constants. We show that all these constraints can be accommodated with fairly reasonable low energy parameters. Finally, in subsection III E we provide predictions for the pion mass dependence of the controversial $f_0(600)$ scalar resonance parameters, which are remarkably stable under the two-loop uncertainties. In addition, we provide predictions for the coupling constant of the ρ and the Kawarabayashi-Suzuki-Riazuddin-Fayyazuddin (KSRF) relation.

A. IAM and mIAM

The ρ and σ resonances appear as poles in $\pi\pi$ scattering partial waves with definite isospin I and angular momentum J, in the $I=1$, $J=1$ and $I=0$, $J=0$ channels respectively. Elastic unitarity implies for these

partial waves and physical values of s:

$$\mathrm{Im}\, t(s) = \sigma(s)|t(s)|^2 \;\Rightarrow\; \mathrm{Im}\, 1/t(s) = -\sigma(s), \qquad (1)$$

where s is the Mandelstam variable and $\sigma(s) = 2p/\sqrt{s}$, p being the center of mass momentum. Consequently, the imaginary part of the inverse amplitude is known exactly. ChPT amplitudes, being an expansion $t = t_2 + t_4 + \cdots$, with $t_k = O(p^k)$, satisfy unitarity only perturbatively:

$$\mathrm{Im}\, t_2 = 0, \quad \mathrm{Im}\, t_4 = \sigma|t_2|^2, \quad \cdots . \qquad (2)$$

Let us recall that t_2 corresponds to a tree level calculation with the leading order (LO) chiral Lagrangian, whereas t_4 contains the one loop diagrams with LO vertices, plus tree level terms from the NLO chiral Lagrangian. The LO Lagrangian has no free parameters, but just m_π and f_π. Higher order Lagrangians contain Low Energy Constants (LECs) that renormalize the loop divergences and whose values contain the information about the underlying theory, QCD. These LECs carry a scale dependence to cancel that of the loop integrals, so that observables are scale independent and finite order by order.

The IAM [4] uses elastic unitarity and the ChPT expansion to evaluate a once subtracted dispersion relation for the inverse amplitude. The analytic structure of $1/t$ consists on a right cut (RC) from threshold to ∞, a left cut (LC) from $-\infty$ to 0, and possible poles coming from zeros of t. The scalar waves vanish at the so called Adler zero, s_A, that lies on the real axis below threshold. Its position can be approximated with ChPT, $s_A = s_2 + s_4 + \cdots$, where t_2 vanishes at s_2, $t_2 + t_4$ vanishes at $s_2 + s_4$, and so on. We can write then a once subtracted dispersion relation for $1/t$, the subtraction point being s_A,

$$\frac{1}{t(s)} = \frac{s - s_A}{\pi} \int_{RC} ds' \frac{\mathrm{Im}\, 1/t(s')}{(s' - s_A)(s' - s)} + LC(1/t) + PC(1/t), \qquad (3)$$

where $LC(1/t)$ stands for a similar integral over the left cut and $PC(1/t)$ is the contribution of the pole at the Adler zero. Note that, as $1/t$ already has a pole at s_A the usual subtraction constant terms are actually part of the pole contribution term.

On the right cut we can evaluate exactly $\mathrm{Im}\, 1/t = -\sigma = -\mathrm{Im}\, t_4/t_2$, as can be read from eqs. (1) and (2). Since the left cut is weighted at low energies we can use ChPT to approximate $LC(1/t) \simeq LC(-t_4/t_2^2)$. The pole contribution $PC(1/t)$ can be safely calculated with ChPT since it involves derivatives of t evaluated at s_A, which is a low energy point where ChPT is perfectly justified. Altogether, we arrive to a modified one-loop IAM (mIAM) formula [4]:

$$t^{mIAM} = \frac{t_2^2}{t_2 - t_4 + A^{mIAM}},$$
$$A^{mIAM} = t_4(s_2) - \frac{(s_2 - s_A)(s - s_2)[t_2'(s_2) - t_4'(s_2)]}{s - s_A}, \qquad (4)$$

where the prime denotes a derivative with respect to s and where we use for s_A in the numerical calculations its NLO approximation $s_2 + s_4$. The standard IAM formula is recovered for $A^{mIAM} = 0$, which is indeed the case for all partial waves except the scalar ones. In the original IAM derivation [2, 3] A^{mIAM} was neglected since it formally yields a higher order contribution and is numerically very small except near the Adler zero. However, if A^{mIAM} is neglected, the IAM Adler zero occurs at s_2, correctly only to LO, is a double zero instead of a simple one, and a spurious pole appears close to the Adler zero. All of these caveats disappear with the mIAM, and the differences between the IAM and the mIAM in the physical and resonance region are less than 1%.

It is important to remark that, in the above derivation, ChPT has *not* been used *at all* for calculations of $t(s)$ for positive energies above threshold. Note that the use of ChPT is well justified to calculate s_A and PC, since these are low energy calculations. ChPT has also been used to calculate the left cut integral, which, despite extending to infinity, is heavily weighted at low energies, which once again justifies the use of ChPT. The approximation of the left cut and the subtraction constants up to a given order in ChPT – with the subtraction point chosen at low energy –, together with the elastic approximation are the only approximations used to derive the IAM from the dispersion relation, but no other model dependent assumptions are made. In particular there are no spurious parameters included in the IAM derivation, but just the ChPT LECs, m_π and f_π.

Remarkably, the simple Eqs.(4) (either the IAM or the mIAM) ensure elastic unitarity, match ChPT amplitudes at low energies, and, using LECs compatible with existing determinations, describe fairly well data up to somewhat less than 1 GeV, generating the ρ, K^*, σ and κ resonances as poles on the second Riemann sheet.

Of course, other unitarization techniques are possible, but in order to improve the NNLO IAM these would imply the use of coupled channels, which are not needed for the σ and the ρ, higher orders of ChPT, which, if available, could be incorporated in a higher order IAM version, or a different approximation of the left cut. For the latter, we can distinguish two possible regions for improvements: either at low energies, where we could systematically include more orders of ChPT, again leading to a higher order IAM version, or at high energies (which are nevertheless suppressed by the subtractions) where the left cut should be modeled introducing more - non ChPT – parameters whose dependence on QCD is not known, or further assumptions beyond those used in the IAM. There is also, of course, an ambiguity on where to choose the subtraction point, but, as shown in [4], different choices contribute to higher order corrections in the subtraction constants and the pole contribution terms, which numerically differ very little from one another.

Finally, there are other unitarization techniques which are very successful and simpler than the IAM. However these can be recast, in the elastic regime, as the IAM

plus further approximations, like dropping crossed and tadpole terms [26] – and therefore keeping a spurious parameter like a cutoff or an unknown subtraction constant to regulate the theory – or keeping just the leading order [5], in which case the ρ cannot be reproduced with natural size parameters (see discussion below). Some of these simpler methods can be easily understood in terms of resummations of particular sets of Feynmann diagrams, but without the said additional simplifications there is no proof that the IAM, and much less so the mIAM, can be obtained from a simple diagrammatic resummation. All these simpler methods are known to provide physical results for the scalars rather similar to the IAM. However, in order to extrapolate to non-physical quark masses one would need additional model dependent assumptions on the behavior of the spurious parameters. For the reasons explained in the last two paragraphs the IAM is the most adequate and complete technique to study the quark mass dependence of the ρ and σ elastic resonances.

For our purposes in sec.III A it is important to remark that it has been shown [5] that the scalars can actually be generated mimicking the LEC, tadpole and crossed channel diagrams by a cutoff of natural size, and thus it is said that scalars are "dynamically generated" from, essentially, meson-meson dynamics (meson loops). In contrast, to generate the vectors, *a precise knowledge of the LECs is needed*, namely, of the underlying, non meson-meson QCD dynamics. As we will see this makes the $\rho(770)$ much more sensitive to the still poorly known two-loop LECs, whereas the sigma is rather stable under such higher order corrections.

Thus, by changing m_π in the IAM amplitudes we can study how the generated ρ and σ poles evolve, so we can predict the dependence of their masses, widths and couplings on m_π. The values of m_π to be considered should lie in the applicability region of ChPT and should allow for some $\pi\pi$ elastic regime. Both criteria would fail above, roughly, $m_\pi \simeq 500$ MeV, which was taken as the upper bound for one-loop calculations in [1]. We will see here that the approach is not reliable much before, namely, around $m_\pi \simeq 300 - 350$ MeV at least.

In [1] the mIAM was used for the ρ and σ chiral extrapolation, because, for the scalar and at high m_π, one resonance pole gets near the IAM spurious pole, a problem that is nicely solved with the mIAM. Nevertheless, in the physical region and near the other generated poles, the differences between IAM and mIAM approaches are almost negligible, even for high pion masses. What we have briefly reviewed is just the NLO, or one-loop, case derived in [4]. For this work we will need the two-loop version of the mIAM that we will explicitly calculate in sect.III below. But first we will show that the predictions obtained in [1] for the chiral extrapolation of the one-loop case are in quite good agreement with recent lattice results on the pion mass dependence of the ρ mass, f_π and isospin 2 scattering length.

II. ONE-LOOP RESULTS

Within the SU(2) ChPT formalism, for $\pi\pi$ scattering only four LECs appear at $O(p^4)$, and are denoted by $l_1^r, \cdots l_4^r$. Since for now we just want to compare the predictions in [1] with lattice results, we will use the same values as in [1]. Namely, we use $10^3 l_3^r = 0.8 \pm 3.8$, $10^3 l_4^r = 6.2 \pm 5.7$ from [6]; and l_1^r and l_2^r are obtained from a mIAM fit to phase shift data up to the resonance region, $10^3 l_1^r = -3.7 \pm 0.2$, $10^3 l_2^r = 5.0 \pm 0.4$. All the LECs are evaluated at $\mu = 770$ MeV.

Let us first compare with lattice results and then we will calculate explicitly the coupling constant of resonances to two pions.

A. Comparison with lattice

Around the time of the publication in [1], several lattice calculations were published providing results for the pion decay constant f_π [8, 12, 14] and also for the $\pi\pi$ scalar isospin 2 scattering length a_{20} [12]. What we will show next is that, despite these lattice results were not used as input in the calculations of [1], they are fairly well described within our one-loop formalism.

In particular, when changing m_π in our amplitudes we have to change accordingly the value of f_π, as it also depends on m_π. Note that, of course, the f_π calculation is not unitarized, but just standard ChPT. However, f_π is an important factor in all our unitarized calculations. Actually, since we are using ChPT up to $O(p^4)$ in the IAM dispersion relations, we evaluate the f_π dependence on m_π to that order. At $O(p^4)$, the only LEC that appears in the m_π dependence of f_π is l_4^r, whose value is fixed here to that given in [6], as commented above. In the top panel of Fig. 1 we compare the resulting one loop dependence of f_π on m_π with some lattice results. The grey area covers the uncertainty in l_4^r only, and one should also recall that lattice uncertainty bars are statistical. We consider the spread of the different lattice groups as an estimate of their systematic errors. With these remarks in mind, we can see that the f_π dependence implemented in our approach is compatible with that calculated from the lattice. Our grey band does not extend beyond $m_\pi = 0.5$ GeV because, at the very least, that is for sure an applicability bound for our calculations. In the next sections, we will see that at those pion masses the two-loop uncertainties are actually too big to make any significant quantitative claim with our method, which we will find reliable only up to roughly $m_\pi \simeq 300 - 350$ MeV, at most.

The $I = 2, J = 0$ $\pi\pi$ partial wave can be calculated with the IAM, and indeed it was included in the fit to phase shift data [1], thus constraining its energy dependence. However, the m_π dependence of a_{20} was not constrained with any input. Of course, it can be easily predicted and is interesting to compare it with the available lattice data as a consistency check of the method. Thus,

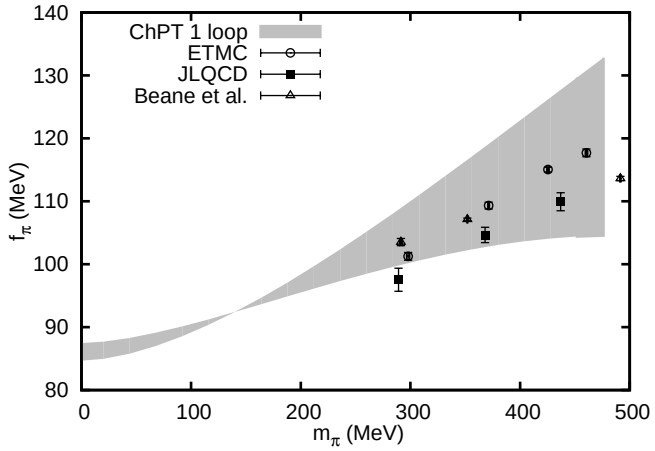

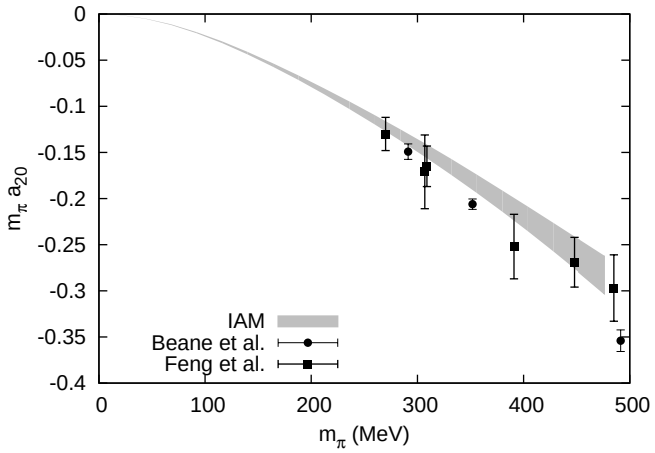

FIG. 1: Top: One loop ChPT and lattice results for the f_π dependence on m_π, but with the l_4^r parameter used in our IAM fits. Lattice points are from [8, 12, 14]. Bottom: IAM and lattice results for the $I = 2, J = 0$ scattering length a_{20} dependence on m_π. Lattice points are from [12, 13].

in the bottom panel of Fig. 1 we show the lattice results for a_{20} compared to our IAM calculation. Once again, one should take into account that the mIAM error band only covers the uncertainties in the one-loop LECs. In view of the figure, and taking into account that our curve is not a fit to these data, we consider that our predictions are in fairly good agreement with these lattice results.

Of course, we could refit our approach including the data in Fig.1, and we would be getting a better agreement, but at this point we only want to check the consistency of our results and that we do not need a fine tuning to describe lattice results, which will be included as input of two-loop fits in the next sections below.

We have thus checked our method for consistency against available lattice results on two quantities other than resonance masses, which we address now. First, let us recall that the mass M and width Γ of a narrow resonance are related to its pole position as $\sqrt{s_{pole}} = M - i\Gamma/2$, and this notation is usually also kept for wide

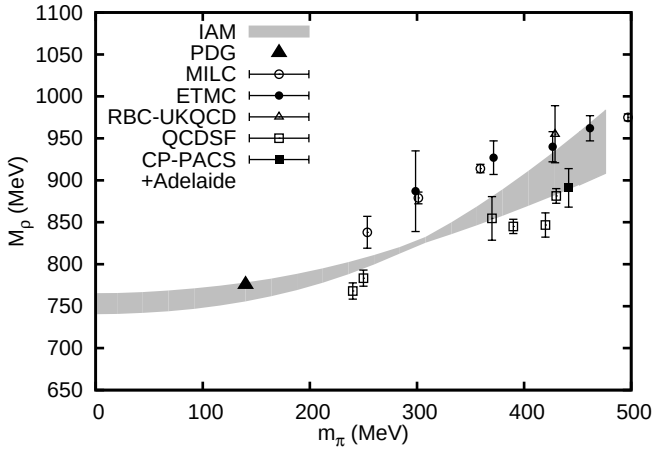

FIG. 2: Comparison of our IAM results for the M_ρ (calculated here as the point where the phase crosses $\pi/2$) dependence on m_π with some recent lattice results [7–11]. The grey band covers only the error coming from the LECs uncertainties.

resonances, as done in [1]. However, lattice calculations do not provide results in the complex plane. For that reason, in this work we will also consider for the $\rho(770)$ the most usual and physically intuitive definition: namely, that the mass of the resonance corresponds to the energy where the scattering phase shift reaches $\pi/2$. This is the value where the modulus of the scattering amplitude shows a peak, and we will thus call it "peak mass". Of course, this definition is only valid for narrow resonances, and is a very good approximation for the ρ, which is the one for which more reliable lattice results exist. For the σ we will stick to the pole mass definition.

Thus, in Fig. 2 we show the results of our IAM calculation of the ρ mass evolution when m_π varies, which is displayed as a grey band that covers the uncertainties in the one-loop fitted LECs only. This behavior agrees nicely with the estimations for the two first coefficients of the M_ρ chiral expansion [15]. This figure is relatively similar to Fig. 3 in [1], except that we plot versus m_π and not m_π^2 and that we have defined the mass as the energy where the phase shift crosses $\pi/2$. This latter choice ensures that the physical ρ mass from the PDG [39] lies within our uncertainty band. In contrast, the "pole" mass would lie somewhat lower. This difference between "pole" and "peak" masses decreases as m_π increases, and they are almost indistinguishable around 350 MeV. Of course, we are now comparing with a compilation of lattice results from different collaborations. Let us remark that due to the finite lattice volume, for some of the lattice results, the minimum energy with which pions are produced is larger than the resulting M_ρ and therefore the resonance has zero width. With these caveats in mind, and in view of the large systematic deviations between different lattice collaborations, one can conclude that our one-loop prediction shows a rather good agreement with the bulk of lattice results.

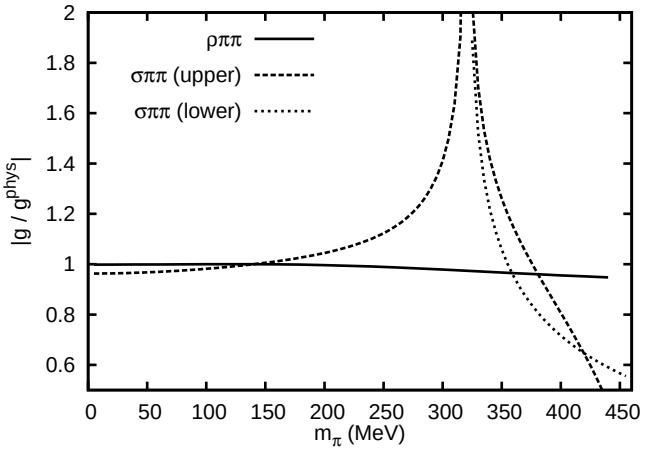

FIG. 3: ρ (continuous line) and σ (dashed line) couplings to $\pi\pi$ evolution with m_π. Since the two conjugate σ poles become two real poles after reaching the real axis, there is a coupling for the pole that moves towards threshold ("up") and another one for the pole moving away ("down").

B. Resonance couplings

In Ref. [1] it was shown that both the ρ and σ widths – calculated with the mIAM from the imaginary parts of the pole positions– decrease as m_π is increased. It was also shown that the decrease in Γ_ρ is largely kinematical, following remarkably well the expected reduction from phase space as M_ρ approaches threshold, whereas the σ width decreases in a quite different way of that provided only by phase space reduction. Following this argument it was concluded in [1] that the effective coupling of the ρ to $\pi\pi$ must be almost m_π independent and that the σ coupling should show a strong m_π dependence. However, we did not perform an explicit calculation of these couplings, and we will provide it here. For elastic amplitudes with a given isospin I and angular momentum J, we can define their coupling g to two pions as

$$g^2 \sim \lim_{s\to s_p} \frac{(s-s_p)t_{IJ}(s)}{p^{2J}}, \qquad (5)$$

where s_p is the position of the resonance pole on the second Riemann sheet, and p is the center of mass momentum. The above definition, if used as such, is very unstable numerically. For that reason we have calculated the residue applying Cauchy's Theorem to a small circle surrounding the pole.

In Fig. 3 we show the results for the couplings. The continuous line shows the $\rho\pi\pi$ effective coupling evolution as m_π changes, defined as in Eq.(5) from the IAM partial wave and normalized to its physical value. As expected, it is almost m_π independent, since it deviates by less than 5% from its original value when changing the pion mass from 139.57 MeV up to 450 MeV.

The results of our explicit calculation thus confirm quantitatively the ρ coupling independence suggested qualitatively in [1]. This result is very relevant because it justifies the constancy assumption made in lattice studies of the $\rho(770)$ width [17].

In contrast, the $\sigma\pi\pi$ coupling, plotted as the dotted line of Fig. 3 shows a strong m_π dependence. The dramatic peak in this curve, around 320 MeV corresponds to the pion mass where, as shown in [1], the two conjugated poles of the sigma meson on the second Riemann sheet join on the real axis below threshold. As the pion mass increases beyond that value, the two poles remain real and we therefore have to plot two different branches. One of these two poles (labeled "lower") stays away from threshold, at least within the mass range of this study. In contrast, the other one (labeled "upper") moves towards threshold and, eventually jumps onto the first Riemann sheet. For the one loop calculation this occurs slightly above $m_\pi = 450\,\mathrm{MeV}$, but we will see that for the two-loop calculations this may occur for pion masses even only slightly above 300 MeV. Let us also remark that it is a nice consistency check to see that, as the pole reaches threshold, the coupling tends to zero, as it is expected from general arguments [18, 19].

As it could be expected, our results both for the $\rho(770)$ and the σ are also in very good agreement with a very recent one-loop calculation using unitarized SU(3) ChPT [16], since the strange quark mass plays a very little role in the $\rho(770)$ and σ values of their masses and widths. Of course, we expect our SU(2) results to be more reliable than those of SU(3) since, as it is well known, the SU(2) ChPT convergence is much better. The small differences with respect to [16] can only be attributed to small differences in the choice of LECs. Actually the SU(2) LECs that we use here were fitted in [1] to pion-pion scattering data only. In contrast, in [16] the SU(3) LECS used there were fitted to the whole elastic meson-meson scattering data below 1 GeV plus some lattice results. The effect of the the kaon loops, which have been integrated out in the large kaon mass limit, is negligible compared to our uncertainties.

III. TWO-LOOP FORMALISM AND RESULTS

In this section we extend our analysis to the next to next to leading order (NNLO), namely, two-loop unitarized ChPT. As we will see, the present knowledge about the two-loop LECs is rather poor. However, it will be enough to obtain sufficiently robust predictions for some observables, particularly those related to the σ meson, and to estimate the size of the uncertainties due to higher order terms in the different parts of the calculation. First of all, of course, we have to rederive the mIAM formalism for the two-loop case.

A. The two-loop mIAM formalism

As we have already commented, instead of the IAM, we need the mIAM in order to describe properly the subthreshold region in the scalar waves. As explained in subsection I A, in the dispersion integral of Eq.(3) we now have to evaluate the left cut and the pole contribution using the $O(p^6)$ expansion of the ChPT amplitudes: $t = t_2 + t_4 + t_6 + ...$ Of course, now the position of the Adler zero has to be evaluated also up to that order, i.e., $s_A \simeq s_2 + s_4 + s_6$. After a tedious calculation along the lines of [4], we arrive at the $O(p^6)$ version of the mIAM:

$$\begin{aligned} t^{mIAM} &= \frac{t_2^2}{t_2 - t_4 + t_4^2/t_2 - t_6 + A^{mIAM}}, \\ A^{mIAM} &= t_4(s_2) - \frac{2t_4(s_2)t_4'(s_2)}{t_2'(s_2)} - \frac{t_4^2(s_2)}{t_2'(s_2)(s-s_2)} \\ &+ t_6(s_2) + \frac{(s-s_2)(s_A-s_2)}{s-s_A}\left(t_2'(s_2) - t_4'(s_2)\right. \\ &\left. - t_6'(s_2) + \frac{t_4'(s_2)^2 + t_4''(s_2)t_4(s_2)}{t_2'(s_2)}\right), \end{aligned} \tag{6}$$

As a technical remark, let us note that we have to introduce an additional subtraction to ensure convergence. Note also that we will now need the second derivative of t_4 with respect to s at s_2. Again, the standard two-loop IAM [3, 23] is recovered for $A^{mIAM} = 0$, which occurs for all waves with $J > 0$. We can now use the $O(p^6)$ mIAM to calculate the chiral extrapolation of the ρ and σ resonance poles, and check the consistency with the $O(p^4)$ results.

B. Two-loop ChPT and the low energy constants

The two-loop $\pi\pi$ SU(2) ChPT scattering amplitude was calculated in [24] and contains six additional LECs. These are denoted $r_1, \cdots r_6$ and their values are poorly known. Moreover, this $O(p^6)$ calculation is expanded in terms of $(m_\pi/f_\pi)^2$, where f_π is the pion decay constant evaluated at the physical value of the pion mass, not in the chiral limit. That is fair enough to describe the physical scattering amplitude, but in order to extract the pion mass dependence of the scattering amplitude one also has to include the $O(p^6)$ ChPT f_π pion mass dependence [29]:

$$\begin{aligned} \frac{f_\pi}{f_0} &= 1 + \frac{m_\pi^2}{f_0^2}(l_4^r - L) + \frac{m_\pi^4}{f_0^4}\left[-\frac{1}{N}\left(\frac{l_1^r}{2} + l_2^r\right)\right. \\ &+ L\left(7l_1^r + 2l_2^r - l_4^r + \frac{29}{12N}\right) - \frac{3}{4}L^2 \\ &\left. - 2l_3^r l_4^r + \frac{1}{N^2}\left(\tilde{r}_f - \frac{13}{192}\right)\right], \end{aligned} \tag{7}$$

where $L = \frac{1}{N}\log\left(m_\pi^2/\mu^2\right)$, $N = 16\pi^2$ and $\tilde{r}_f$ is the relevant combination of $O(p^6)$ LECs that appears in f_π, poorly known once again. For that reason, we will use lattice data on f_π to stabilize it in our fits.

TABLE I: Sample of LECs: First row: Roy-Steiner eqs. SU(3) analysis of πK scattering. Second and third rows: K_{l4} analysis to $O(p^4)$ and $O(p^6)$, respectively. Naively, we have combined quadratically the SU(3) LECs errors there. Fourth row: Roy Eqs. analysis with uncertainties from imaginary parts and unknown $O(p^6)$ LECs combined quadratically. Fifth row: Roy Eq. analysis of low-energy $\pi\pi$ scattering up to two loops, whose errors "only account for the noise seen in their calculations". Last row, values used in [1] with the IAM. All LECs are evaluated at the scale $\mu = 770$ MeV

Analysis	$10^3 l_1^r$	$10^3 l_2^r$	$10^3 l_3^r$	$10^3 l_4^r$
$O(p^4)$ [22]	-4.9 ± 0.6	5.2 ± 0.1	–	17 ± 10
$O(p^4)$ [30]	-4.5	5.9	2.1	5.7
$O(p^6)$ [30]	-3.3 ± 2.5	2.8 ± 1.1	1.2 ± 1.7	3.5 ± 0.6
$O(p^6)$ [20]	-4.0 ± 2.1	1.6 ± 1.0	–	–
$O(p^6)$ [21]	-4.0 ± 0.6	1.9 ± 0.2	0.8 ± 3.8	6.2 ± 1.3
IAM [1]	-3.7 ± 0.2	5.0 ± 0.4	0.8 ± 3.8	6.2 ± 5.7

Let us now remark that the two-loop leading log contributions, which are numerically dominant at low energies, do not depend on the r_i constants, but just on the one-loop l_i^r. For this reason it is well known that the values of the $l_1^r \cdots l_4^r$ $O(p^4)$ LECS can vary sizably between the $O(p^4)$ and $O(p^6)$ analysis, as it is shown in Table I, where we quote the LECs obtained in several works [20–22, 30]. Let us remark that error bars in the $l_1^r \cdots l_4^r$ usually correspond to the statistical uncertainty ("noise") in the input, but there are other large systematic sources of uncertainty that are most likely dominant. Hence, it should not be surprising that some of the $O(p^6)$ LECs deviate somewhat from the estimates when taking into account leading log terms from $O(p^8)$ and higher orders, as we will do with the IAM.

Finally, it has been shown [25] that the LECs can be understood as the effective couplings that result from integrating out heavy fields. Indeed, most one-loop LECs values are saturated by vector resonance exchange, like the $\rho(770)$, but note that the σ plays a little role, if any, in the actual values of the LECs. These resonance saturation estimates have also been extended to the $O(p^6)$ LECs [24], but these are very uncertain and are customarily assigned a 100% uncertainty. We have collected them in Table II, together with some other estimates coming from dispersive analysis of pion-pion scattering [21].

At this point we want to make clear that the LECs do *not* depend on the quark mass. This is a rather obvious statement for people familiar with ChPT but, when presenting in conferences and workshops [31, 32] previous results from Ref. [1] or partial preliminary results from this work, we have found that people get confused since we have just stated that the l_i^r are saturated by resonance exchange – like ρ exchange – but we have shown that the ρ mass depends on the quark mass. The reason for this confusion is that resonance saturation is usually

interpreted as a $\sim 1/M_R^2$ contribution to the l_i^r, with M_R the physical mass of a resonance. However it is actually a $\sim 1/M_{R0}^2$ contribution, with M_{R0} the resonance mass in the chiral limit, namely $M_R^2 = M_{R0}^2 + O(m_\pi^2)$. Numerically, using M_R instead of M_{R0} makes a small difference – neglected when obtaining LECs estimations – but is incorrect in terms of ChPT. A term like $\sim 1/M_R^2$ coming from integrating out a heavy resonance should be re-expanded as $\sim 1/M_{R0}^2(1 + O(m_\pi^2/M_{R0}^2))$. The first term contributes to l_i^r, but the next $O(m_\pi^2)$ term counts as a higher order in ChPT and therefore does not contribute to the same order as l_i does. The same occurs to all orders, so, as stated above, *the LECs do not have to be readjusted when the mass of higher resonances change with m_π. They do not depend on the quark mass.*

C. Resonance sensitivity to LECs

After reviewing briefly the standard ChPT two-loop calculation, we can now use it to generate the $\rho(770)$ and $f_0(600)$ resonances, for which we use the mIAM. Thus, we show once again in Table I the LECs we obtained in the one-loop IAM fit in [1], which are fairly compatible with the non-unitarized determinations, lying roughly in between the one and the two-loop bulk determinations. Naively, this could correspond to the fact that the one-loop IAM, reproduces not only the one-loop ChPT expansion but also the numerically relevant s-channel two-loop diagrams.

At this point it is important to recall the different role that LECs play in the generation of the $\rho(770)$ and the σ resonances. In particular, it has been shown that the σ can be easily generated within the chiral unitary approach [5] from the leading order ChPT – which only depends on f_π and m_π – and a natural cutoff, whereas that is not feasible for the $\rho(770)$, which needs the input from the one-loop LECs [26]. This is also understood from the $1/N_c$ behavior of these resonances [27, 28]: namely, the $\rho(770)$ behaves nicely as a $\bar{q}q$ state when generated from the IAM – a N_c dependence due to the the $1/N_c$ behavior of the leading LECs. In contrast, the σ does not behave *predominantly* as a $\bar{q}q$ and this dependence is mostly due to logarithmic terms, which are independent of the LECs and are generated from meson loops. This explains why the σ, despite being lighter than the ρ, is not contributing so sizably to the value of the low energy constants. In summary, the terms containing LECs play a crucial role in the generation and location of the ρ pole in the IAM, but not so much for the σ. This is due to the fact that to generate the ρ we need the input from the underlying QCD dynamics of a $\bar{q}q$ state, and we expect this to occur to all orders in ChPT, whereas the sigma is dominated by the scale f_π [5] and should depend much more mildly on the underlying QCD dynamics encoded in the LECs.

This is actually what we find when we look for the m_π dependence of the ρ pole with the $O(p^6)$ IAM; its behavior is quite unstable under the large uncertainties of the $O(p^6)$ LECs. If we leave completely free the $O(p^6)$ parameters within their huge estimated uncertainties, we cannot make any two-loop prediction for the $\rho(770)$. For this reason, at two loops we will fit not only experimental data but also the LECs values. In addition, by fitting the experimental data only, as was done in [1], one constrains mostly the combinations of $O(p^6)$ chiral parameters that govern the energy dependence. However, one cannot expect to constrain the $O(p^6)$ LECs combinations that govern the pion mass dependence that is of interest here. Fortunately, as we have seen in previous sections, there is a large amount of lattice data on the pion mass dependence of the $\rho(770)$ mass, the $I = 2$ scattering length and f_π, which can be used to constrain further the $O(p^6)$ LECs and will be included in our fits. Once this is done, we will obtain predictions for the m_π dependence of the ρ coupling and width, as well as on all the $f_0(600)$ parameters, which is where the most interesting discussion is still going on.

D. Unitarized two-loop constrained fits

We have thus fitted the mIAM to the elastic pion-pion scattering phase shifts shown on the left column of Fig.4. Let us remark that we have fitted data up to 1 GeV for the $(1,1)$ and $(2,0)$ waves and up to 800 MeV for the $(0,0)$ channel; beyond that energy the effects of the $f_0(980)$ are important and cannot be reproduced with our single channel formalism. There are, of course, coupled channel unitarization formalisms [5, 37], which are very successful and generate the $f_0(980)$ among other resonances, but they lie beyond the scope of this work, mostly because of their simpler treatment of the left cut – if dealing with it at all–, or their dependence on additional parameters, all of which can introduce further model dependences.

In addition, in order to constrain further the LECs that govern the pion mass dependence, we have also fitted the lattice results shown in Figs.1 and 2 in previous sections, although only up to a pion mass of 350 MeV.

Still, we have 11 parameters to fit, and even with these constraints, because of the large correlations between parameters, during the fitting procedure some LECs can take values very far from their typical ones, even of different order of magnitude, for tiny improvements in the data χ^2. For that reason, we have also considered an averaged χ^2_{LECs} term as a constraint for our fits, that measures how far the LECs are from some reference values that we provide in Table II. To further constrain the fit, we will also require the ρ mass and width leading $1/N_c$ scaling to follow a $\bar{q}q$ pattern, so we also consider a $\chi^2_{\rho-\bar{q}q}$ measure, as described in [28], to constrain the ρ behavior to that of a $\bar{q}q$. Note that uncertainties for $N_c = 3$ are of the order of 30%, but this constraint becomes stricter as N_c grows. Nevertheless, we will never apply this constraint for N_c larger than 20, since oth-

erwise the theory would become weakly interacting and the whole unitarization procedure would loose sense, as repeatedly explained in [31, 38].

In summary, we are considering several χ^2-like functions that, when smaller or close to 1, ensure a good description of each feature described above: χ^2_{data}, $\chi^{2\,lattice}_{M_\rho}$, $\chi^{2\,lattice}_{a_{20}}$, $\chi^{2\,lattice}_{f_\pi}$ $\chi^2_{\rho-\bar{q}q}$ and χ^2_{LECs}. The problem is that many of these are not really well defined χ^2 functions in the statistical sense. The reasons are that some uncertainties we use are theoretical (as for the $1/N_c$ behavior), and that some sets, both for real data or lattice, are incompatible with each other and we have to guess some systematic uncertainty of the order of the difference between different sets. In addition, the number of "data points" to be fitted for each feature is very different, and we could get a bad description of one feature with few "data" at the expense of a tiny improvement on another feature with more "data", but affected by systematic errors crudely estimated. Thus, there is not a single fit of data and lattice minimizing the sum of all χ^2 functions, since we do not know how to weight each one of them against the others. We are nevertheless presenting four different "fits" A, B, C and D where we have imposed that each one of the χ^2 should be relatively close or smaller than 1. This is still quite a strong constraint, and ensures, as we will see in Fig. 4, that all features are fairly well described up to the applicability region. Thus, in Table II we show the parameters of four different fits, which, as seen in Fig.4, cover the data and lattice results fitted up to pion masses of 350 MeV. In particular, we show the M_ρ dependence on m_π versus the lattice data, the $IJ = 00, 11, 20$ partial waves, as well as the a_{20} and f_π dependence on m_π compared with lattice results. Note that these fits tend to prefer the somewhat stronger M_ρ pion mass dependence found by the MILC [7], ETMC [8] and RBC-UKQCD [9] collaborations. The leading $1/N_c$ behavior of the ρ pole is also shown in Fig. 5.

Fit	Fit A	Fit B	Fit C	Fit D	Reference
$10^3 l^r_1$	-5.0	-4.7	-5.0	-4.0	-3.3 ± 2.0
$10^3 l^r_2$	1.7	0.95	1.7	1.24	1.9 ± 1.0
$10^3 l^r_3$	0.82	0.82	-6.0	0.82	0.82 ± 3.8
$10^3 l^r_4$	6.5	4.96	3.5	6.5	6.2 ± 2.0
$10^4 r_1$	-0.6	-1.0	-0.7	-0.6	-0.6
$10^4 r_2$	1.3	1.3	3.7	1.5	1.3
$10^4 r_3$	-1.7	-0.29	2.7	-3.3	-1.7
$10^4 r_4$	2.0	4.2	2.8	0.95	-1.0
$10^4 r_5$	2.0	2.3	2.0	1.7	1.5
$10^4 r_6$	-0.56	-0.98	-0.5	-0.7	0.4
$\tilde{r}_f$	-3.4	-1.8	-2.3	-4.6	0

TABLE II: LECs for the $O(p^6)$ fits A, B, C and D and the reference values we use in χ^2_{LECs}. For the $O(p^4)$ LECs we have used values that cover the different sets in Table I, whereas for the $O(p^6)$ LECs we show estimates from [21, 24]

In view of the different χ^2 per data points (abbreviated as $\chi^2/(\#\text{points})$) that we list in Table III and will describe in detail below, we consider that fits A and D

$\chi^2/(\#\text{points})$	Fit A	Fit B	Fit C	Fit D
δ_{00} Sol. B [35]	0.8	1.1	0.5	0.6
δ_{00} Sol. C [35]	5.6	1.1	2.6	5.7
δ_{00} below 400 MeV	0.87	0.8	0.9	1.0
δ_{11}	1.2	1.6	0.7	0.7
δ_{20}	0.2	1.0	0.3	0.4
$M_\rho^{lattice}$	0.77	0.68	0.88	1.35
$a_{20}^{lattice}$	0.2	4.0	0.06	0.2
$f_\pi^{lattice}$	1.4	1.1	0.6	0.8
N_c	1.4	0.6	1.2	1.5
LECs	1.5	3.8	3.2	1.4

TABLE III: $\chi^2/(\#\text{points})$ for each feature fitted. See main text for details of the χ^2 calculation.

are the best ones, particularly because their LECs are quite compatible with the values of the $O(p^4)$ LECs and reasonably close to the crude expectations for the $O(p^6)$ ones. The difference between them is that fit A describes better the M_ρ pion mass dependence – even up to very high pion masses – and not so well the a_{20} scattering length, whereas fit D does the opposite. In addition, we provide two other fits to illustrate the uncertainties. First, on fit B we try to force the softer M_ρ pion mass dependence found by the CP-PACS-Adelaide [10] and QCFSF [11] collaborations. Note that this fit then prefers the less negative phase shift data of the $(I, J) = (2, 0)$ channel, an, as a consequence it does not describe very well the mass dependence of the a_{20} scattering length. Also, the agreement with the LECs estimates is worse than for fit A, as seen in Table II. In addition we are showing the results for fit C, which is very similar to A and D up to pion masses of 300 MeV, but shows a rather dramatic drop of the ρ mass above 350 MeV. It is a general feature of our fits that they can be made reasonably compatible with data up to 350 MeV, but beyond that point they can start diverging widely for not very large changes in the LECs. That is the reason why we consider that our approach is not reliable beyond a pion mass of 300 to 350 MeV, depending on the observable.

Before proceeding to the next section we want to provide, for each feature included in our fit, the χ^2 per number of data points. Of course, in view of the clear incompatibilities of different sets of data for a given quantity – from experiment or lattice –, we have either added some systematic uncertainty to cover different sets, or fitted some particular subsets of data, as we detail next. Let us emphasize that, since we use the IAM and have made several approximations on its derivation, we are obviously not aiming at precision. As it is seen in Fig.4 the spread of our four fits covers roughly the different data points.

The chaotic situation with the (0,0) phase shifts above 450 MeV (obtained from $\pi N \to \pi\pi N$ experiments) is well known and very visible in Fig.4. Even the same CERN/Munich experiment [35] provides 5 different analysis (A, B, C, D and E) incompatible with each other. Among them, data sets B and C have been shown to be the ones that satisfy better several dispersive constraints

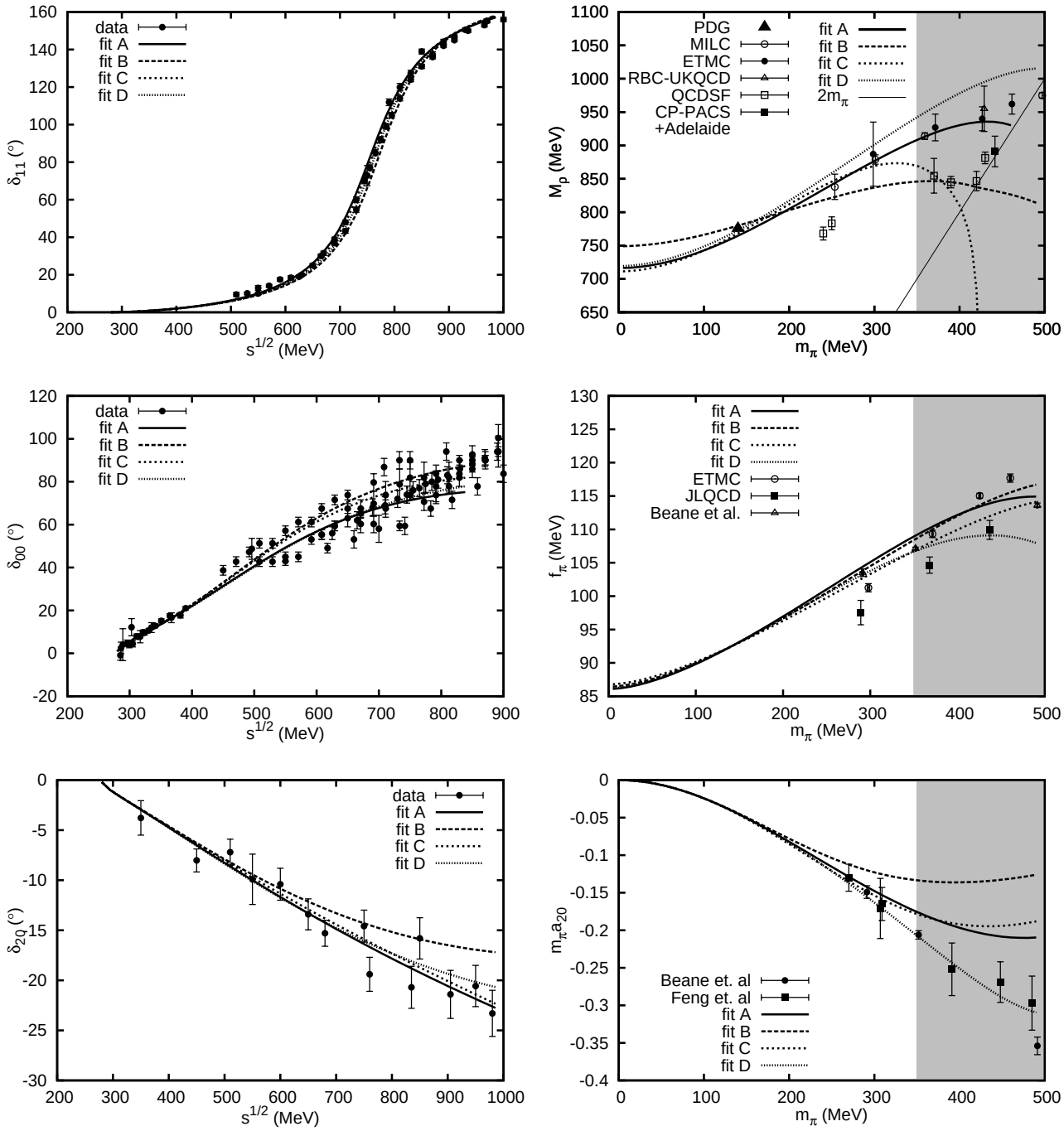

FIG. 4: Different fits to physical $\pi\pi$ scattering phase shifts δ_{IJ} and lattice results on the ρ mass, f_π and the a_{20} scattering length. For the lattice results, we have not extended our fits to the grey area ($m_\pi > 350\,\text{MeV}$, although it is displayed to show how the fits deteriorate, or not, beyond 350 MeV. The phase shift data comes from [33–35] and the lattice results from [7–14].

[36]. Thus, we have added linearly 2 degrees of systematic uncertainty to the points of these two sets – not much given the huge incompatibilities. In Table III we provide the resulting $\chi^2/(\#\text{points})$ for each fit with respect to the data sets B and C in [35]. Note that, for each fit, at least one of the two experimental sets is well described, i.e., with $\chi^2/(\#\text{points}) < 1$. If we wanted $\chi^2/(\#\text{points}) \simeq 1$ for all data sets plotted in Fig.4 simultaneously, we would have to add 5 degrees as a systematic error, which again would not be much taking into account that differences between data sets in the 700 to 800 MeV region can be as high as 15 degrees. Fortunately, the K_{l4} decay data below 400 MeV [34] is of much better quality, but is easily reproduced by our fits without the need to add system-

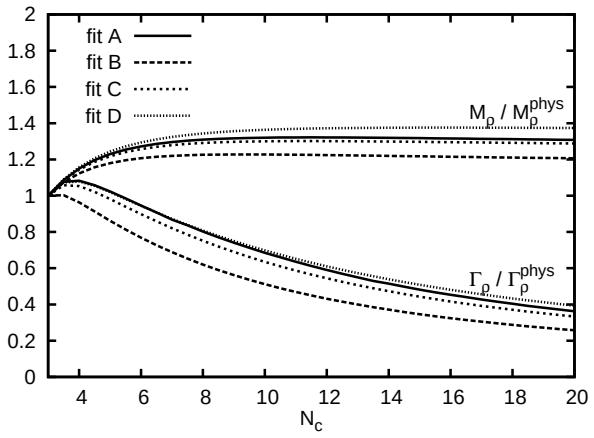

FIG. 5: N_c dependence of $\rho(770)$ mass and width for the different fits described in the text.

atic uncertainties as seen also in Table III.

The fits to other quantities are less complicated. Despite they look relatively close, the two sets of $(I, J) = (1, 1)$ $\pi\pi$ scattering phase shifts are not compatible, since they provide tiny statistical errors only. Their difference is of the order of two degrees, which once again we have added linearly as a systematic error. Concerning the $(2, 0)$ wave, once more it is clear that there are incompatible sets of data, and we have added the same 2 degrees of systematic uncertainty. The resulting χ^2/(#points) for all our fits are given in Table III. Note that, once again, fit B can be used to differentiate the $(2, 0)$ "low data" set from the "high data" set and that it does not reproduce so well as the others the physical ρ shape.

Concerning the lattice predictions for the ρ mass, there is also an obvious conflict between different collaborations, with differences in the M_ρ value as high as 70 MeV. Hence, the χ^2/(#points) given in Table III has been calculated for the points with m_π below 350 MeV, adding a systematic uncertainty of 35 MeV. Note that if we took into account data up to $m_\pi = 400\,\mathrm{MeV}$, the χ^2/(#points) would have been 0.95, 0.93, 0.99 and 2.1 for fits A to D, respectively.

In the case of the f_π lattice results, different collaborations have points clustered sufficiently close in groups of three to estimate a systematic uncertainty as half the difference between the highest and lowest data point, which is added linearly to the statistical errors. The resulting χ^2 for each fit with this prescription is shown in Table III. Note that we find some difficulty in describing the JLQCD results simultaneously with the other features.

The leading order $1/N_c$ behavior of the ρ has been adjusted to be exactly that of a pure $q\bar{q}$ state. This is believed to be a very good approximation, although given its large physical width it may easily have some small $\pi\pi$ component, that we neglect. Using the χ^2 definitions and estimating the uncertainty to be exactly $1/N_c$ times the leading term, as explained in [28], we find the averaged χ^2 for the ρ as a pure $q\bar{q}$ state shown in Table III.

The last quantity that we have fitted is the (2,0) scattering length, where we find one data point right at $m_\pi = 350$ MeV and four other points below. There are two collaborations and their points are relatively consistent with each other. Thus, and despite the large differences between different collaborations for other observables, we have not added any systematic error to these points. For the four points strictly below 350 MeV we show the χ^2/(#points) for each fit in table III. Once again fit B has serious problems describing this observable, but note that it describes better the "high data" set of (2,0) phase shifts. If we now include the point at $m_\pi = 350\,\mathrm{MeV}$ with its tiny uncertainty, the χ^2/(#points) of all fits except fit D grow beyond 4.5.

It is clear that our fits A, C and D give a very good general description of, at least, one set of data for each observable up to 300 MeV, but not so good up to 350 MeV, where they start deviating from each other also for the M_ρ quark mass dependence. For that reason we will consider our IAM approach to be valid only up to, roughly, the 300 to 350 MeV region. This is, of course a crude estimate and varies from one observable to another.

Finally, concerning the χ^2_{LECs}, let us remark that to calculate it we use the reference values given in Table II. Since the values of the r_i $O(p^6)$ parameters come from resonance saturation estimates (with resonances of angular momentum smaller than 2), we have assumed that they are only correct in the order of magnitude and therefore have a 100% uncertainty. For all fits, most of the deviations come from the $O(p^6)$ LECs, which are the worst known. Note that, in general, but particularly in this case, fits A and D are the ones with better χ^2 and that is the reason why we consider them as our best fits. Fits B and C are just given for illustration of different scenarios and to show that the *predictions* that we will detail next are robust even allowing for larger uncertainties or deviations from our best fits.

E. Predictions from the fits

Once we have obtained a relatively good description of the data and existing lattice results on certain observables, we will now use these three fits to obtain *predictions for other observables*. In general, the spread between our curves should be considered as a naive indication of our systematic uncertainties.

1. *The ρ width and coupling*

First of all, in Table IV we provide the values of the ρ pole position, s_ρ, in the lower half plane of the second Riemann sheet and its coupling to two pions defined from the (1,1) partial wave as

$$g_\rho^2 = -16\pi \lim_{s\to s_{\rm pole}} (s - s_\rho)\; t_{11}(s) \frac{3}{4\,p^2}, \qquad (8)$$

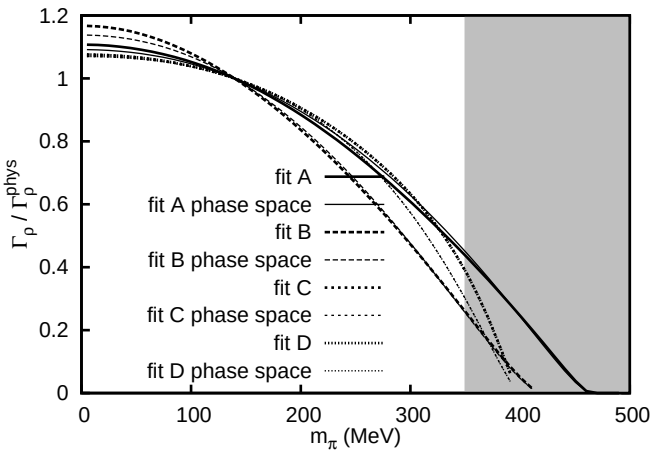

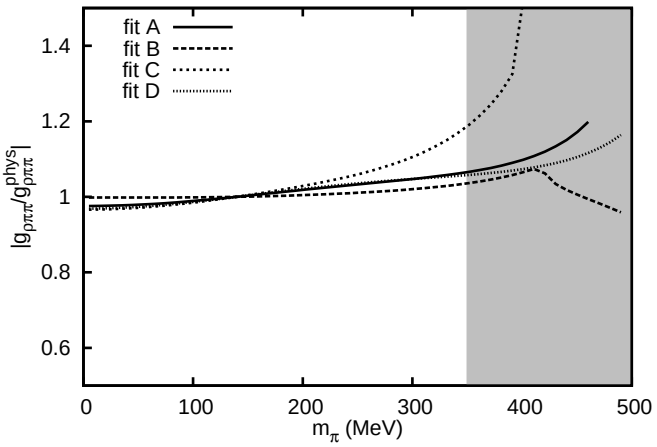

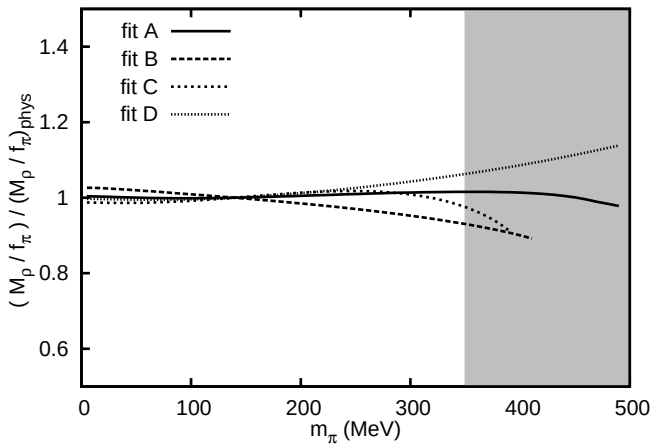

FIG. 6: Predictions for the pion mass dependence of ρ parameters from the IAM two-loop fits described in the text and Fig.4. Top: We show the rho width from each IAM fit together with the behavior expected only from phase-space variation due to the changing ρ mass. Middle: the ρ coupling. Bottom: the M_ρ/f_π ratio. The last two are remarkably independent of the quark or pion mass, which ensures that the KSRF relation is not spoiled within the applicability region of our approach.

	$\sqrt{s_\rho}$ (MeV)	$\lvert g_\rho \rvert$
fit A	$754 - i\,74$	6.1
fit B	$772 - i\,71$	5.9
fit C	$759 - i\,72$	6.0
fit D	$763 - i\,71$	5.9

TABLE IV: Values of the ρ pole position in the lower half plane of the second Riemann sheet and $\rho\pi\pi$ couplings for the different fits described in the text.

where the normalization factors are chosen to recover the usual expression for the two-meson width of the ρ:

$$\Gamma_\rho = |g_\rho|^2 \frac{1}{6\pi} \frac{|\mathbf{p}|^3}{M_\rho^2}. \tag{9}$$

If we approximate $M_\rho = \mathrm{Re}\,\sqrt{s_\rho}$ in the above equations, and we use the value of the coupling in Table IV, we find that the width of the ρ for fits A to D are 149, 144, 145 and 142 MeV, respectively, to be compared with the PDG value of 149 ± 1 MeV. [39]. A rather good description, given the approximation, the quality of the data, and that we only provide central values.

On the top panel of Fig.6 we show the evolution of the ρ width for the two-loop unitarized ChPT fits described in the text and Fig.4. Although hard to see because they are almost overlapping, we provide, together with the result of each fit, the expected variation from phase space due to the change in M_ρ only, assuming a constant $\rho - 2\pi$ coupling in a Breit-Wigner form. As it happened in the one-loop case [1], we see that this constancy assumption of the ρ coupling is a very good approximation, so that this feature is rather robust under higher order ChPT corrections when fitting to data and lattice results on f_π and a_{20}.

Moreover, in the middle panel of Fig.6, we show the actual two-loop IAM calculation of the coupling from the residues of the amplitude at the resonance pole. We can see that it is rather independent of the pion mass up to $m_\pi \simeq 350$ MeV. Namely, fit B barely changes at all, fits A and D change by roughly 5% and only fit C changes by 15%, to be compared with the factor of 2.5 times that the pion mass is increased from its physical value up to 350 MeV. Actually, this corresponds to an increase in the quark mass larger than a factor of 6. Thus, the relatively weak dependence of the $\rho-2\pi$ coupling on the quark mass is confirmed at two loops. This is of particular relevance to some lattice calculations that have assumed a constant coupling in studies of the ρ width [17]. Nevertheless, this prediction of M_ρ with the quark mass is limited to pion masses below roughly 350 MeV, and more uncertain within our two-loop approach than at one-loop, as we see from the spread between different fits. Actually, for the less favored fit C we see up to a 15% variation, but note that the M_ρ mass in this fit C starts behaving rather weird around 350 MeV, and most likely it is, very roughly speaking, only reliable up to the region between 300 to 350 MeV, depending on the observable.

Finally for the $\rho(770)$, we show in the lower panel of

	$\sqrt{s_\sigma}$ (MeV)	$\lvert g_\sigma\rvert$ (MeV)
fit A	$453 - i\,265$	3.4
fit B	$474 - i\,248$	3.5
fit C	$466 - i\,245$	3.3
fit D	$453 - i\,271$	3.5
H. Leutwyler et al.[41]	$441^{+16}_{-8} - i(272^{+9}_{-12.5})$	$3.31^{+0.35}_{-0.15}$
R. García-Martín *et al.* [40]	$474 \pm 6 - i(254 \pm 4)$	3.58 ± 0.03
R. Kaminski *et al.*[42]	$442 - i290$	2.47 ± 0.45
J.A. Oller [43]	$(443 \pm 2) - i(216 \pm 4)$	2.97 ± 0.04

TABLE V: Values of the σ pole position in the lower half plane of the second Riemann sheet and $\sigma\pi\pi$ couplings for the different fits described in the text and some references in the literature.

Fig.6 the evolution of the M_ρ/f_π ratio, which comes almost independent of m_π in all of our two-loop fits. This ratio is not really a prediction, since we have fitted both M_ρ and f_π to lattice data. However, it is of particular interest for the well known KSRF relation [44], which provides an striking connection between the $\rho - 2\pi$ coupling and the M_ρ/f_π ratio:

$$g^2_{\rho\pi\pi} \simeq M^2_\rho/8f^2_\pi, \tag{10}$$

and holds fairly well for the physical values of these constants. Since we have just checked the almost constancy of $g_{\rho\pi\pi}$, then, an almost constant M_ρ/f_π ratio as found in Fig.6 means that the KSRF relation also holds rather nicely, at least within our applicability region. This corroborates the one-loop results already found in unitarized SU(3) ChPT [16].

2. *The σ parameters*

Let us turn to the predictions for the pion mass dependence of the σ or $f_0(600)$ scalar resonance, whose nature is still very controversial. As we did with the ρ we provide first the values of the resulting σ pole positions and couplings in Table V, obtained as follows:

$$g^2 = -16\pi \lim_{s\to s_\sigma} (s - s_\sigma)\; t_{00}(s). \tag{11}$$

For comparison we also provide in the last rows of Table V results from other works in the literature. Let us remark that, without using the recent and very precise K_{l4} decay data [34], the σ pole was obtained more than fourteen years ago at $\sqrt{s_\sigma} = 440 - i\,245\,\mathrm{MeV}$, with the single channel one loop IAM in [3].

The $O(p^6)$ results are in quantitative agreement with the $O(p^4)$ ones for pion masses lower than about 300 MeV. For instance, as the quark mass is increased, the relative growth of the σ mass, defined as the real part of the σ pole position, is slower than the pion mass growth, but still somewhat faster than for the ρ mass.

As we saw for the one-loop case in previous sections and in [1], as the pion mass grows, since the sigma mass grows slower, its width becomes narrower and narrower, and its two conjugate poles approach the real axis. But contrary to the ρ case, it is possible to have poles below threshold on the second Riemann sheet, and the σ conjugate poles actually meet at some point on the real axis below threshold. If the pion mass keeps on increasing, both poles stay on the real axis, but one moves very little, remaining at masses lower than threshold, whereas the other one increases its mass, until it eventually jumps to the first Riemann sheet. All these features occur once again at two loops and this double real pole structure is nicely seen in the top panel of Fig.7 as a double branch for each fit.

Let us remark that the appearance of two branches is not an artifact of the IAM, but is a general feature of scattering theory of scalar amplitudes with poles close to threshold [49], also seen in other contexts [50]. It is just the way scalar poles approach to threshold as one changes the features of the interaction. Namely, there are no restrictions on where a scalar pole should be on the real axis below threshold *on the second Riemann sheet*, except that poles appear in conjugate pairs out of the real axis, or on the real axis below threshold. In the first case, they obviously have the same "mass", but if this pair reaches the real axis, the two poles no longer have to be conjugated and hence the double branch is a general feature. In contrast, all non-scalar waves have centrifugal p^{2J} factors relevant around threshold, that force their second sheet poles to reach the real axis precisely at threshold [49] where one of them jumps into the first sheet whereas the other stays in the second, as it happens here with the $\rho(770)$.

The IAM, of course, not only reproduces this general feature, but also provides an estimate of the pion mass where this apparent splitting occurs, which is not generic, but a specific value due to the QCD dynamics underlying the properties of the lightest scalar meson.

Let us remark that all our fits are very consistent with each other for the σ, despite their differences for the ρ behavior. As explained above, this is due to the fact that in the generation of the σ the chiral loops play a dominant role. At NLO these are independent of the LECs, and at NNLO they only depend on the $O(p^4)$ LECs, but not on the r_i. Therefore the σ avoids most of the largest uncertainties that affect the ρ and, as a consequence, the results for the σ are much more robust. There are however, some quantitative differences with the one-loop results in [1]: for instance, the point where the two conjugate poles of the σ meet on the real axis occurs for m_π masses about 20 MeV lower; namely, at $m_\pi = 280 - 310$ MeV for the different two-loop fits versus $300 - 330\,\mathrm{MeV}$ for the one-loop description. This is a rather small correction to the one-loop result and confirms the robustness of our results for the σ, even under higher loop corrections, at least up to $m_\pi \simeq 300 - 350$ MeV, depending on the observable. However, for higher pion masses the quantitative spread is much larger, although the four fits yield the same qualitative predictions for the poles in the two branches. Closely related to the decrease of the "split-

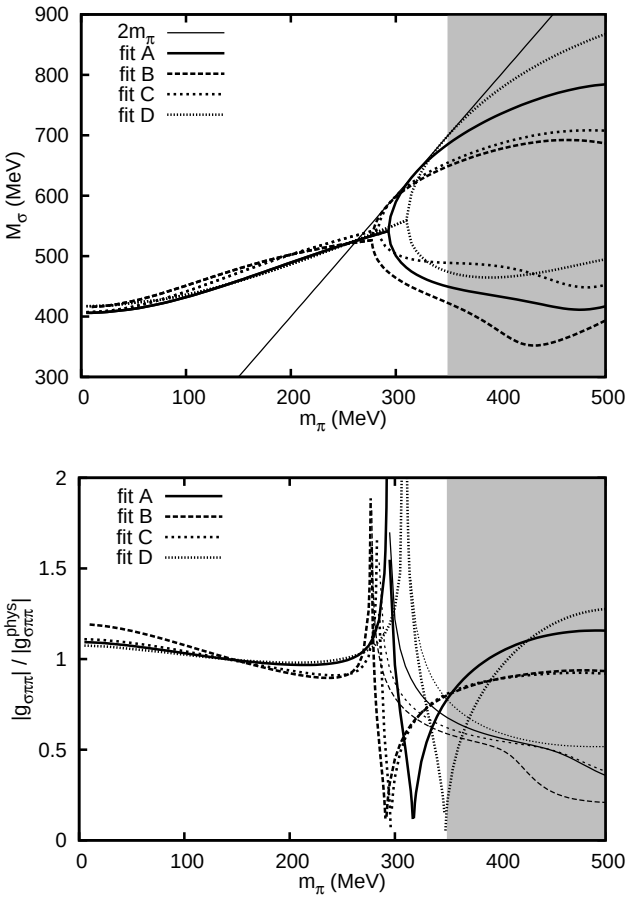

FIG. 7: Predictions for the σ from the IAM two-loop fits described in the text and Fig.4. Note they are remarkably stable despite the differences between fits for the ρ. We show as a grey area the region where $m_\pi > 350$ MeV, which marks the applicability bound of the approach. Top: we show the predicted pion mass dependence for the σ pole mass. Note the appearance of two branches around 300 MeV, as explained in the text. Bottom: we show the dependence of the σ coupling to two pions, which, as explained in the text, is rather strong particularly as the pion mass approaches the value where the two conjugate poles on the second Riemann sheet reach the real axis. For each fit, the thick line corresponds to the upper branch and the thin one to the lower branch.

ting point" is the fact that the pole of the "upper branch" reaches the threshold faster than in the one-loop case as the pion mass grows. Note that the threshold variation corresponds to the line labeled $2m_\pi$ in the figure, that the upper branches of all fits touch very soon after the two branch splitting, around $m_\pi \simeq 290-350$ MeV, versus $m_\pi \simeq 460$ MeV for the one loop calculation in [1].

The relevance of these results is that, when the upper branch pole reaches threshold, it jumps into the first Riemann sheet, and becomes a usual bound state. (One might wonder if the dispersion relation for the IAM applies now that there is a pole on the first Riemann sheet, but note that the IAM derivation is obtained from dispersion relations for the *inverse amplitude*, so that this pole on the first Riemann sheet is a zero for the inverse amplitude and therefore does not alter the analytic structure). Our two-loop results seem to indicate that a conventional bound state – not a virtual one– might be found for pion masses higher than $290-350$ MeV, contrary to the 460 MeV we found at one-loop, which as we have seen was for sure outside the region where our approach is reliable. This is in qualitative agreement with some recent lattice results in [45], where they seem to find a bound state for $m_\pi \simeq 325$ MeV. Let us nevertheless recall the caveats raised from the very authors of [45], since they cannot calculate accurately the width, and some possibly relevant contributions – mainly the disconnected contractions– have not been included in the calculation. Other lattice studies [46] have also suggested the existence of a "tetraquark" component for $m_\pi \simeq 180-300$ MeV. Let us note, however, that the binding energy of the states we find at two-loops seems to grow faster with the pion mass than for the one-loop case and on the lattice. However, this occurs already in the region $m_\pi > 350$ MeV, where we do not consider our approach reliable and the uncertainties are huge as seen by the spread of the fits in Fig.7. Unfortunately, other relevant lattice calculations for the σ [47, 48], lie beyond our reach.

Finally, in the lower panel of Fig.7 we show our results for the $\sigma-2\pi$ coupling, obtained from the residue of the second Riemann sheet pole – or poles when there are two branches. The qualitative behavior is similar to the one-loop case shown in Fig.3, with a dramatic rise up to a peak that occurs at the pion mass where the two conjugate poles meet on the real axis. From that value onwards we thus have to draw two branches for each fit, and it can be noticed that the coupling for one of these branches reaches zero. This corresponds to the pion mass where the upper branch pole reaches the 2π threshold. The fact that at threshold the coupling goes to zero is in good agreement with the well known result in [18]. Actually, this can be checked analytically because, as shown in [19], the coupling is inversely proportional to the energy derivative of the one-loop function which is divergent at threshold.

IV. SUMMARY

Using the IAM, which is based on analyticity, elastic unitarity and ChPT, we generate the poles associated to the ρ and σ resonances without any assumption on their existence or nature. The IAM implements the pion mass dependence of observables through the subtraction constants up to a given order in ChPT. Thus, we can predict the dependence of the ρ and σ pole positions on m_π, as done in [1]. Here we present new results that were missed in the previous paper.

First, using the one-loop formalism, we have made a comparison of our previous results with some recent lattice data, showing that they are compatible. We have

also calculated the m_π dependence of the $\rho\pi\pi$ and $\sigma\pi\pi$ effective couplings, calculated from the pole residues, finding that the $\rho\pi\pi$ coupling is almost m_π independent, whereas the $\sigma\pi\pi$ coupling shows a strong m_π dependence.

Finally, we have extended to two-loops the modified Inverse Amplitude Method formalism to account properly for Adler zeros, which has been applied then to the $O(p^6)$ calculation. Although no robust predictions can be made for the ρ mass, mostly due to the large uncertainties in the low energy constants, we have been able to describe the elastic scattering phase shift data and lattice results on f_π and a_{20} with several fits with fairly reasonable values for such low energy constants, and the correct $\bar{q}q$ leading $1/N_c$ behavior of the ρ.

With these fits we have obtained relatively robust predictions for other ρ observables and all σ parameters, at least up to $m_\pi \simeq 300 - 350\,\mathrm{MeV}$. In particular, we have confirmed the relatively weak dependence of the $\rho - 2\pi$ coupling and the approximate validity of the KSRF relation. Concerning the sigma, whose results are much more robust than for the ρ since it has a much weaker dependence on the ChPT low energy constants, we have confirmed the appearance of two virtual poles for sufficiently high pion masses. One of these poles becomes a virtual state for m_π between, roughly, 300 and 350 MeV. We hope these results could be of use as a guideline for future extrapolations of lattice results down to physical quark mass values.

Acknowledgments

We thank C. Hanhart for useful discussions. Work partially supported by Spanish Ministerio de Educación y Ciencia research contracts: FPA2007-29115-E, FPA2008-00592 and FIS2006-03438, U.Complutense/Banco Santander grant PR34/07-15875-BSCH and UCM-BSCH GR58/08 910309. We acknowledge the support of the European Community-Research Infrastructure Integrating Activity Study of Strongly Interacting Matter (acronym HadronPhysics2, Grant Agreement n. 227431) under the Seventh Framework Programme of EU.

[1] C. Hanhart, J. R. Pelaez and G. Rios, Phys. Rev. Lett. **100**, 152001 (2008)
[2] T. N. Truong, Phys. Rev. Lett. **61** (1988) 2526. Phys. Rev. Lett. **67**, (1991) 2260; A. Dobado et al., Phys. Lett. **B235** (1990) 134.
[3] A. Dobado and J. R. Peláez, Phys. Rev. D **47** (1993) 4883; Phys. Rev. D **56** (1997) 3057.
[4] A. Gomez Nicola, J. R. Pelaez and G. Rios, Phys. Rev. D **77**, 056006 (2008)
[5] J. A. Oller and E. Oset, Nucl. Phys. A **620**, 438 (1997) [Erratum-ibid. A **652**, 407 (1999)].
[6] J. Gasser and H. Leutwyler, Annals Phys. **158**, 142 (1984).
[7] C. W. Bernard *et al.*,Phys. Rev. D **64**, 054506 (2001)
[8] Ph. Boucaud *et al.* [ETM Collaboration], Phys. Lett. B **650**, 304 (2007)
[9] C. Allton *et al.* [RBC and UKQCD Collaborations], Phys. Rev. D **76**, 014504 (2007)
[10] C. R. Allton *et al.*Phys. Lett. B **628**, 125 (2005)
[11] M. Gockeler *et al.*[QCDSF Collaboration], [arXiv:hep-lat/0810.533q7].
[12] S. R. Beane *et al.*Phys. Rev. D **77**, 014505 (2008)
[13] X. Feng, K. Jansen and D. B. Renner, Phys. Lett. B **684**, 268 (2010)
[14] J. Noaki *et al.*, arXiv:0810.1360 [hep-lat].
[15] P. C. Bruns and U.-G. Meißner, Eur. Phys. J. C **40** (2005) 97.
[16] J. Nebreda and J. R. Pelaez., Phys. Rev. D **81**, 054035 (2010)
[17] S. Aoki *et al.* [CP-PACS Collaboration], Phys. Rev. D **76**, 094506 (2007).
[18] S. Weinberg, Phys. Rev. **130**, 776 (1963). V. Baru, J. Haidenbauer, C. Hanhart, Yu. Kalashnikova and A. E. Kudryavtsev, Phys. Lett. B **586**, 53 (2004).
[19] D. Gamermann, J. Nieves, E. Oset and E. Ruiz Arriola, Phys. Rev. D **81**, 014029 (2010)
[20] L. Girlanda, M. Knecht, B. Moussallam and J. Stern, Phys. Lett. B **409**, 461 (1997)
[21] G. Colangelo, J. Gasser and H. Leutwyler, Nucl. Phys. B **603**, 125 (2001)
[22] P. Buettiker, S. Descotes-Genon and B. Moussallam, Eur. Phys. J. C **33**, 409 (2004). S. Descotes-Genon and B. Moussallam, Eur. Phys. J. C **48**, 553 (2006).
[23] J. Nieves, M. Pavon Valderrama and E. Ruiz Arriola, Phys. Rev. D **65**, 036002 (2002)
[24] J. Bijnens, G. Colangelo, G. Ecker, J. Gasser and M. E. Sainio, Nucl. Phys. B **508**, 263 (1997) [Erratum-ibid. B **517**, 639 (1998)]
[25] G. Ecker, J. Gasser, A. Pich and E. de Rafael, Nucl. Phys. B **321**, 311 (1989). J. F. Donoghue, C. Ramirez and G. Valencia, Phys. Rev. D **39**, 1947 (1989).
[26] J. A. Oller, E. Oset and J. R. Pelaez, Phys. Rev. Lett. **80** (1998) 3452, Phys. Rev. D **59** (1999) 074001
[27] J. R. Pelaez, Phys. Rev. Lett. **92**, 102001 (2004)
[28] J. R. Pelaez and G. Rios, Phys. Rev. Lett. **97**, 242002 (2006)
[29] J. Bijnens, Prog. Part. Nucl. Phys. **58**, 521 (2007)
[30] G. Amoros, J. Bijnens and P. Talavera, Nucl. Phys. B **602**, 87 (2001)
[31] J. R. Pelaez, J. Nebreda and G. Rios, New Frontiers in QCD 2010, Yukawa International Program for Quark-Hadron Sciences (YIPQS), January 18 (Mon) - March 19 (Fri), 2010 Yukawa Institute for Theoretical Physics, Kyoto, Japan. arXiv:1007.3461 [hep-ph]. To appear in Progress of Theoretical Physics
[32] J. R. Pelaez, C. Hanhart, J. Nebreda and G. Rios, arXiv:1003.0364 [hep-ph]. G. Rios, A. G. Nicola, C. Hanhart and J. R. Pelaez, AIP Conf. Proc. **1030**, 268 (2008) [arXiv:0803.4318 [hep-ph]]. G. Rios Marquez, A. Gomez Nicola, C. Hanhart and J. R. Pelaez Sagredo, PoS E

FT09, 043 (2009) [arXiv:0905.3489 [hep-ph]].
[33] S. D. Protopopescu *et al.*, Phys. Rev. D **7**, 1279 (1973). P. Estabrooks and A. D. Martin, Nucl. Phys. B **79**, 301 (1974). W. Hoogland *et al.*, Nucl. Phys. B **126**, 109 (1977). M. J. Losty *et al.*, Nucl. Phys. B **69**, 185 (1974). N. B. Durusoy *et al.*, Phys. Lett. B **45**, 517 (1973).
[34] L. Rosselet *et al.*, Phys. Rev. D **15**, 574 (1977). S. Pislak *et al.* [BNL-E865 Collaboration], Phys. Rev. Lett. **87**, 221801 (2001). J. R. Batley *et al.* [NA48/2 Collaboration], Eur. Phys. J. C **54** (2008) 411.
[35] G. Grayer *et al.*, Nucl. Phys. B **75**, 189 (1974).
[36] J. R. Pelaez and F. J. Yndurain, Phys. Rev. D **71**, 074016 (2005)
[37] A. Gomez Nicola and J. R. Pelaez, Phys. Rev. D **65**, 054009 (2002). J. R. Pelaez, Mod. Phys. Lett. A **19**, 2879 (2004) F. Guerrero and J. A. Oller, Nucl. Phys. B **537**, 459 (1999) [Erratum-ibid. B **602**, 641 (2001)] J. Nieves and E. Ruiz Arriola, Phys. Lett. B **455**, 30 (1999) J. A. Oller, E. Oset and J. R. Pelaez, Phys. Rev. Lett. **80** (1998) 3452; Phys. Rev. D **59** (1999) 074001
[38] J. R. Pelaez and G. Rios, arXiv:0905.4689 [hep-ph]; J. R. Pelaez and G. Rios, *In the Proceedings of 11th International Conference on Meson-Nucleon Physics and the Structure of the Nucleon (MENU 2007), Julich, Germany, 10-14 Sep 2007, pp 157* [arXiv:0711.4223 [hep-ph]]; J. R. Pelaez, AIP Conf. Proc. **892**, 72 (2007) [arXiv:hep-ph/0612052].
[39] K. Nakamura et al. (Particle Data Group), J. Phys. G 37, 075021 (2010)
[40] F. J. Yndurain, R. Garcia-Martin and J. R. Pelaez, Phys. Rev. D **76** (2007) 074034
[41] H. Leutwyler, AIP Conf. Proc. **1030**, 46 (2008) [arXiv:0804.3182 [hep-ph]]. I. Caprini, G. Colangelo and H. Leutwyler, Phys. Rev. Lett. **96**, 132001 (2006)
[42] R. Kaminski, G. Mennessier and S. Narison, Phys. Lett. B **680**, 148 (2009).
[43] J. A. Oller, Nucl. Phys. A **727**, 353 (2003).
[44] K. Kawarabayashi and M. Suzuki, Phys. Rev. Lett. **16**, 255 (1966). Riazuddin and Fayyazuddin, Phys. Rev. **147**, 1071 (1966).
[45] S. Prelovsek, T. Draper, C. B. Lang, M. Limmer, K. F. Liu, N. Mathur and D. Mohler, arXiv:1005.0948 [hep-lat]. S. Prelovsek, C. B. Lang, M. Limmer, D. Mohler, T. Draper, K. F. Liu and N. Mathur, PoS **LAT2009**, 103 (2009) [arXiv:0910.2749 [hep-lat]].
[46] N. Mathur *et al.*, Phys. Rev. D **76**, 114505 (2007)
[47] M. G. Alford and R. L. Jaffe, Nucl. Phys. B **578**, 367 (2000)
[48] T. Kunihiro, S. Muroya, A. Nakamura, C. Nonaka, M. Sekiguchi and H. Wada, Nucl. Phys. Proc. Suppl. **186**, 294 (2009) [arXiv:0809.3879 [hep-lat]]. T. Kunihiro, S. Muroya, A. Nakamura, C. Nonaka, M. Sekiguchi and H. Wada [SCALAR Collaboration], Phys. Rev. D **70**, 034504 (2004)
[49] C. Hanhart, R. L. Jaffe, J.R. Peláez and G. Ríos, in preparation.
[50] F. Cannata, J. P. Dedonder and L. Lesniak, Phys. Lett. B **207**, 115 (1988). F. Cannata, J. P. Dedonder and L. Lesniak, Z. Phys. A **334**, 457 (1989). R. Kaminski, L. Lesniak and B. Loiseau, Eur. Phys. J. C **9**, 141 (1999) A. Patkos, Z. Szep, P. Szepfalusy, Phys. Rev. **D66**, 116004 (2002). D. Fernandez-Fraile, A. Gomez Nicola and E. T. Herruzo, Phys. Rev. D **76**, 085020 (2007)